Applied Surface Science 357 (2015) 1830–1835

Contents lists available at ScienceDirect

Applied Surface Science

journal homepage: www.elsevier.com/locate/apsusc

Highly efficient industrial large-area black silicon solar cells achieved by surface nanostructured modification

Ping Li[a], Yi Wei[a], Zengchao Zhao[a], Xin Tan[b], Jiming Bian[a], Yuxuan Wang[a], Chunxi Lu[c], Aimin Liu[a,c,*]

[a] School of Physics & Optoelectronic Engineering, Dalian University of Technology, Dalian, 116024, China
[b] Jinzhou Huachang Photovoltaic Technology Co., Ltd., Jinzhou, 121000, China
[c] College of New Energy, Bohai University, Jinzhou, 121013, China

ARTICLE INFO

Article history:
Received 28 July 2015
Accepted 6 October 2015
Available online 9 October 2015

Keywords:
Solar cell
Black silicon
Nanostructure
TMAH modification

ABSTRACT

Traditional black silicon solar cells show relatively low efficiencies due to the high surface recombination occurring at the front surfaces. In this paper, we present a surface modification process to suppress surface recombination and fabricate highly efficient industrial black silicon solar cells. The Ag-nanoparticle-assisted etching is applied to realize front surface nanostructures on silicon wafers in order to reduce the surface reflectance. Through a further tetramethylammonium hydroxide (TMAH) treatment, the carrier recombination at and near the surface is greatly suppressed, due to a lower surface dopant concentration after the surface modification. This modified surface presents a low reflectivity in a range of 350–1100 nm. Large-area solar cells with an average conversion efficiency of 19.03% are achieved by using the TMAH treatment of 30 s. This efficiency is 0.18% higher than that of standard silicon solar cells with pyramidal surfaces, and also a remarkable improvement compared with black silicon solar cells without TMAH modifications.

1. Introduction

Surface texturing and antireflection coating on the front surface are known to be very important to reduce the surface reflection and thereby enhance the efficiency of solar cells. Conventionally, a random pyramidal structure formed by wet anisotropic potassium hydroxide (KOH) etching combined with surface antireflection coatings (ARCs) like silicon nitride (SiN_x) based on interference is the industrial method used to reduce the reflection of monocrystalline silicon surface [1,2]. However, the SiN_x ARCs deposited on pyramidal structures works only in a narrow spectral range, around 600 nm, and at small angles of incident photons [2–5]. Recently, the black silicon has drawn great attention for nearly ideal photo-absorption across the solar spectrum. The near-zero reflection is obtain by forming the layer with gradually varying refractive index between the air and silicon surface, which is due to the fact that the surface nanostructures are smaller than the incident light wavelength [6–8]. Several methods have been used to fabricate black silicon, including metal-assisted etching [9,10], laser-induced etching [11], reactive-ion etching [12] and electro-chemical etching [13]. In the past, several authors reported improvements in the conversion efficiency of P-type black silicon solar cells. Oh et al. reported 18.2% efficient silicon solar cells on 0.8081 cm^2 float zone (FZ) material, without any antireflection coating layer [14]. Wang et al. presented a 0.92 cm^2-large p-type black silicon solar cells passivated with ALD Al_2O_3 with an efficiency of 18.2% [15]. Our group has previously developed a 17.3%-efficient $156 \times 156\,mm^2$-large black silicon solar cells using metal-nanoparticle-assisted chemical etching without any antireflection coating layer [16].

The black silicon solar cell structure has potential for achieving high efficiencies in mass production for nearly ideal photo-absorption across the solar spectrum. However, at present, the efficiency of "black silicon" solar cells is far lower than the commercially available silicon solar cells with the same process except the surface texture method, which is due to increasing surface recombination and Auger recombination as a result of the large surface area and high doping concentration [14,16]. In this paper, the nanotextured front surface, fabricated using Ag nanoparticles after anisotropic KOH etching, is used to reduce the reflectance of silicon surface. The tetramethylammonium hydroxide (TMAH) is added to modify the surface of nanotextured silicon and control the dopant concentration of the emitter. We optimize the process

* Corresponding author at: School of Physics & Optoelectronic Engineering, Dalian University of Technology, Dalian, 116024, China. Tel.: +86 411 84709285; fax: +86 411 84709285.
E-mail address: pv_lab@dlut.edu.cn (A. Liu).

http://dx.doi.org/10.1016/j.apsusc.2015.10.035
0169-4332/

for large-area mono-crystalline solar cell with nanotextured surface, and achieved a conversion efficiency up to 19.03% for a large $156 \times 156\,mm^2$ mono-crystalline solar cell with nanotextured surface.

2. Experimental

As base material, we used $156 \times 156\,mm^2$-large p-type Czochralski (CZ) silicon wafers with resistivity of 1–3 Ω cm and thickness of $200 \pm 10\,\mu m$. After the saw damage removal, all wafers were immersed into aqueous alkaline solutions with KOH (2 wt%) and IPA (2 wt%) at 80 °C for 25 min to form pyramidal structures. After the pyramid-texturing process, the wafers were arranged as back-to-back and immersed into 5 wt% hydrofluoric acid (HF) solution for 30 s and then immersed in deionized (DI) water. Thus, etching resulted in formation of the nanostructure only on the front surface of the wafers. The Ag nanoparticles were electroless-deposited on the silicon surface by immersing the wafer in 0.001 mol/L $AgNO_3$ and 1 vol% HF solution for 90 s. Then the wafer covered by Ag nanoparticles was immersed in a mixed solution of 10 vol% HF and 2 vol% hydrogen peroxide (H_2O_2) and DI water for 25 s to form the nanostructure silicon surface. Afterward, the wafers were immersed into the solution containing NH_4OH:H_2O_2:DI in a 1:1:5 volume ratio volume for 5 min to remove Ag nanoparticles. After clean the wafer, phosphorus diffusion was carried out in a standard industrial diffusion furnace with optimized process and the edge isolation etching was made by reactive ion etching. The phosphosilicate glass (PSG) layer, formed during diffusion, was removed by 5 wt% HF solution. Subsequently, a 0.05% TMAH solution was used for treatment for 30 s or 60 s to modify the nanostructures and reduce the surface phosphorus doping concentration. The SiN_x coating was deposited by plasma enhanced chemical vapor deposition (PECVD). The front and back metallization of passivated black silicon wafers were carried out using standard screen-printing with Ag-paste and Al-paste respectively, followed by co-firing in a lamp-heated belt furnace. In addition, we also produce some traditional pyramid-textured silicon solar cells with standard production process. The complete cell fabrication process flow is shown in Fig. 1. Finally, we produced four kinds of silicon solar cells: traditional pyramid-textured silicon solar cells as reference (group R), nanotextured solar cells without any modification (group S1), nanotextured solar cells with 30 s TMAH modification (group S2) and nanotextured solar cells with 60 s TMAH modification (group S3).

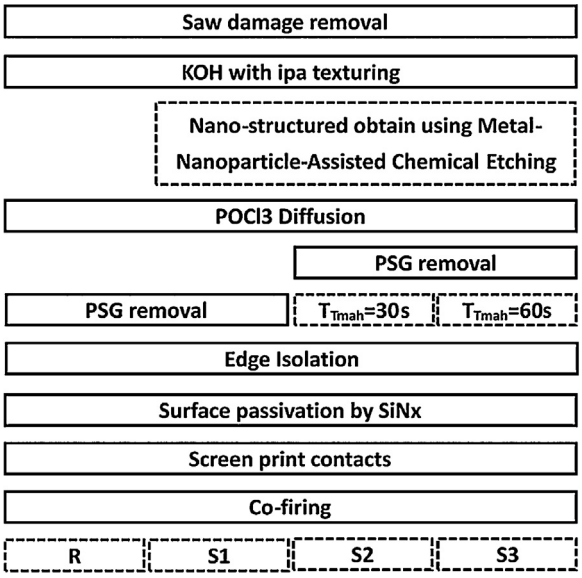

Fig. 1. Processing sequences of our four solar cells presented in Table 1. The dashed boxes highlight the steps that were different in the four process flows.

The surface morphology of black silicon was analyzed using a Hitachi S-4800 field emission scanning electron microscope (FESEM), and the silicon surface reflection was measured with a Varian Cary 6000i spectrometer using an integrating sphere. The passivated wafers were characterized by quasi-steady-state photoconductance (QSSPC) instrument (WCT-120 by Siton Consulting) at an injection level of $\Delta n = 10^{15}\,cm^3$. The quantum efficiencies and photovoltaic conversion efficiencies of these solar cells were tested by Quality Supervision & Testing Center of Chemical and Physical Power Sources of Ministry of Information Industry.

3. Results and discussion

For comparison, the cross-sectional SEM images of the Si wafers subjected to KOH texturing and Ag-assisted etching, and that have modified nanostructures are both presented. Fig. 2(a) is a SEM image of pyramid-textured silicon obtained by etching in alkaline solution. Fig. 2(b) shows the SEM image of nanostructure of black silicon without any modification. It can be seen that the nanopores with a depth of 150–250 nm and a diameter less than 50 nm are formed on the pyramid-textured surface. As shown in Fig. 2(c–d), a majority of the pores of the nanotextured silicon surface modified by 30 s TMAH treatment are about 80 nm in depth and 150–250 nm in diameter, as for the surface modified by 60 s TMAH, the depth of the pores decreased to less than 50 nm and the diameter increased to 300–400 nm. It can be seen that the nanotextured surface area decreases with the TMAH modification because of the reduction in the depth and increase in the pore diameter.

Fig. 3(a) shows the reflectance of pyramid-textured silicon surface, nanotextured silicon surface after 30 s TMAH modification, nanotextured silicon surface after 60 s TMAH modification and nanotextured silicon surface without any modification. The reflectance of the nanotextured silicon wafers are apparently lower than that of the pyramid-textured silicon wafer among the whole wavelength range. The solar-spectrum-weighted average reflectance in the entire wavelength range between 350 and 1100 nm, is 11.3% and 3.9% for pyramid-textured and nanotextured Si wafer, respectively. This is a consequence of the equivalent to a graded index of refraction between air and silicon wafer, when the nanotextured structures are smaller than the wavelength of incident light [6–10]. The average reflectance of nanotextured Si wafer is increased to 6.89% and 9.14% after TMAH treatment for 30 s and 60 s, respectively. It is a high reflectance for the so-called “black silicon”, but it is still much smaller than the reflectance of the pyramid-textured silicon.

Fig. 3(b) shows the reflectance of wafers after the phosphorus diffusion and passivation. SiN_x film was still applied as the passivation coating and further ARCs combination with nanostructures on surface, resulting in reduced reflectance. We found that the SiN_x film based on quarter-wave-length layers deposited on pyramided silicon wafer perform well only in the wavelength range between 550 and 700 nm (<3.5%) and the average reflectance is 5.33% in the wavelength range between 350 and 1100 nm. The SiN_x coating also reduced the reflectance of nanotextured silicon wafers. The average reflectance in the wavelength range between 350 and 1100 nm was 3.78% and decreased to 2.16% after the SiN_x film was deposited. The average reflectance of the nanotextured wafer subjected to TMAH modification for 30 s and 60 s was further reduced to 3.51% and 4.58%, respectively. We found that the wafers exhibit a low reflectance because of the combination of the SiN_x films and the nanotextured silicon.

The effective carrier lifetime and the emitter saturation current for the wafer were used to characterize the influence of the surface

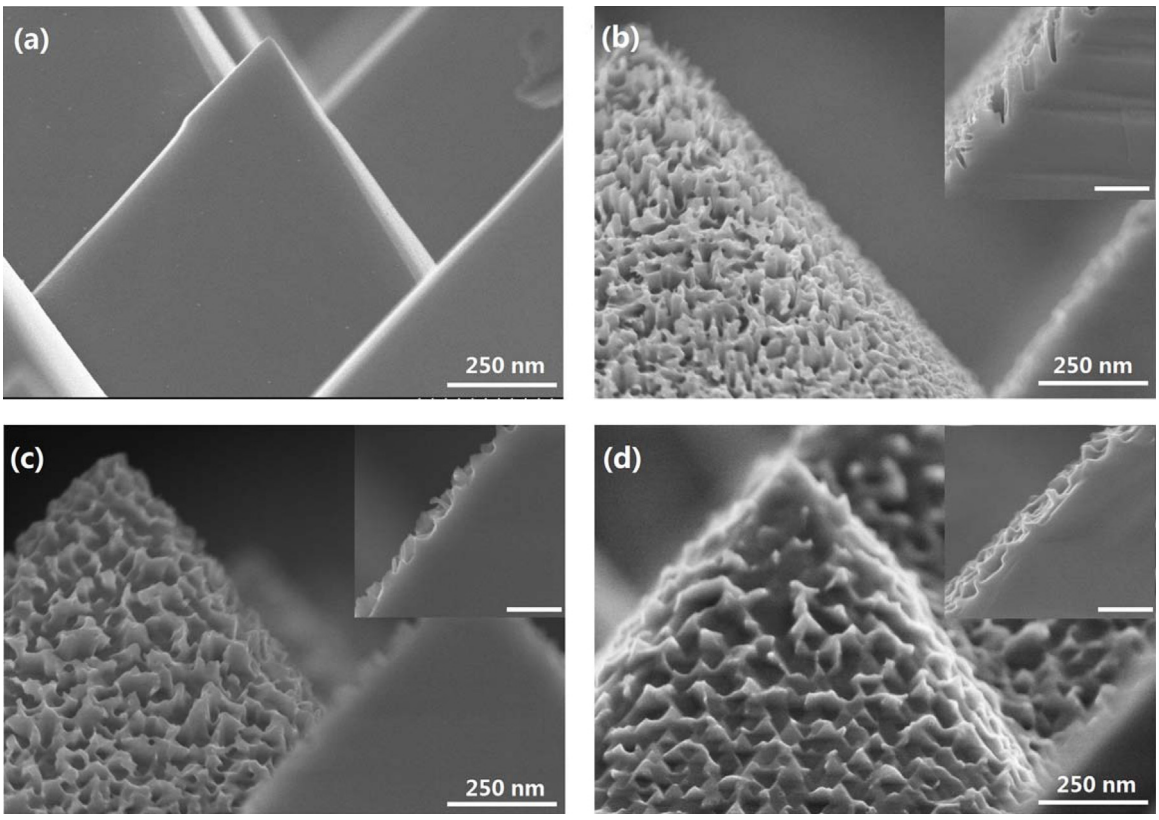

Fig. 2. (a) SEM images of silicon with pyramidal surface. (b) SEM images of silicon with nanotextured surface. (c) SEM images of silicon with nanotextured surface and additionally subjected to TMAH modification for 30 s. (d) SEM images of silicon with nanotextured surface and additionally subjected to TMAH modification for 60 s. The enlarged SEM images of nanopores structures are shown in the insets of b, c, and d (scale bars, 250 nm).

modification with TMAH solution. The test wafers with phosphorus diffusion and SiN_x passivation on both sides were utilized in the measurements of the effective carrier lifetime. Here, we introduce an enlargement area factor, defined as A_{Nano}/A_{Micro}, where A_{Nano} is the effective area of the nanotextures and A_{Micro} is the area of pyramid surface [14]. Fig. 4(a) shows how the effective carrier lifetime increases with the TMAH modification time. At an injection level of $10^{15}\,cm^{-3}$, the lifetime of nanotextured wafer was only 16.74 μs. The lifetimes of wafers were increased to 35.76 μs, 42.0 μs, 45.93 μs and 49.83 μs after etching in TMAH solution for 15 s, 30 s, 45 s and 60 s, respectively. An significantly increase in the effective carrier lifetime was observed, probably as a result of the decrease in the surface area and the suppression of carrier recombination at the emitter region due to the lower dopant concentration.

The effective lifetime for samples can be expressed as follows [17,18]:

$$\frac{1}{\tau_{eff}} - \frac{1}{\tau_{Auger}} = \frac{1}{\tau_{SRH}} + \left[J_{0e(front)} + J_{0e(back)}\right] \frac{(N_A + \Delta n)}{qn_i^2 W} \quad (1)$$

where, τ_{Auger} and τ_{SRH} is the bulk Auger lifetime and bulk Shockley–Read–Hall (SRH) lifetime, respectively. N_A is the dopant density of the wafer, Δn is the excess carrier concentration, n_i is the intrinsic carrier density and W is the wafer thickness. $J_{0e(front)}$ and $J_{0e(back)}$ are the saturation current densities of the front and back emitter regions, respectively.

J_{0e} can be calculate by the derivative of the $(\tau_{eff} - \tau_{Auger})$, provided that the measurement is taken in high injection where τ_{SRH} is constant. In the case of double side nanotextured, diffused and passivated samples, $J_{0e} = J_{0e(front)} = J_{0e(back)}$. So J_{0e} can be calculate by [19,20]:

$$J_{0e} = \frac{qn_i^2 W}{2} \frac{d}{d\Delta n} \left(\frac{1}{\tau_{eff}} - \frac{1}{\tau_{Auger}} \right) \quad (2)$$

Fig. 4(b) shows the saturation current density of nanotextured wafer with and without TMAH modification. It can be seen that the J_{0e} decrease with the modification time within 60 s. The value of J_{0e} decreased sharply at modification time 15 s, and then decreased with further increasing the modification time. The J_{0e} of nanotextured sample was 754 fA/cm^2, and then decreased to 420 fA/cm^2, 322 fA/cm^2, 285 fA/cm^2 and 270 fA/cm^2 after 15 s, 30 s, 45 s and 60 s TMAH modification. The decrease of J_{0e} indicates that lower recombination in emitter region or surface.

The emitter can be defined as a virtual surface positioned at the edge of the depletion region, and emitter recombination can be considered as a special case of surface recombination (S_{eff}) [20]:

$$S_{eff} = S_{eff}^F = S_{eff}^B \approx J_{0e} \left(\frac{N_A + \Delta n}{qn_i^2} \right) \quad (3)$$

S_{eff} as function of the modification time is shown in Fig. 5, S_{eff} can be counted as follows [14]:

$$S_{eff} = \frac{A_{Nano}}{A_{Micro}} S_{loc} \quad (4)$$

where S_{loc} is the local effective surface recombination velocity, which includes recombination at the surface and the doped region near the surface. If the effective surface recombination velocity is independent of the enlargement in the surface area, S_{loc} of samples without TMAH modification and with different modification time will be similar. Fig. 5 shows the S_{eff} and S_{loc} as function of different

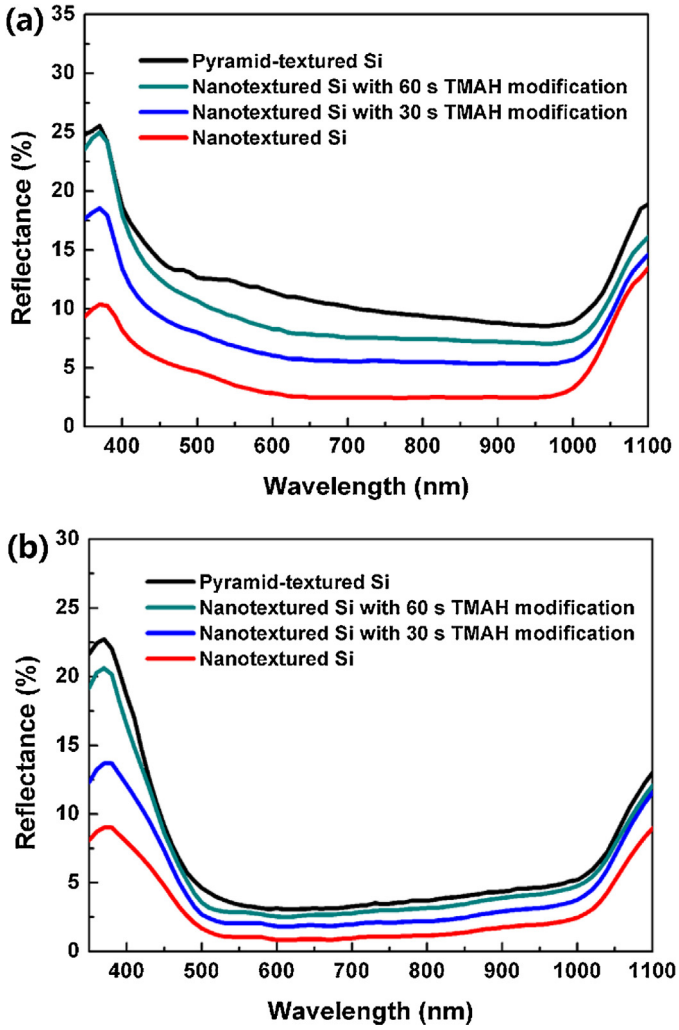

Fig. 3. Reflectance vs. wavelength curves: (a) pyramid-textured silicon, nanotextured silicon, nanotextured silicon with 30 s TMAH modification, and nanotextured silicon with 60 s TMAH modification. (b) Passivated by SiN_x using the substrate sample in (a).

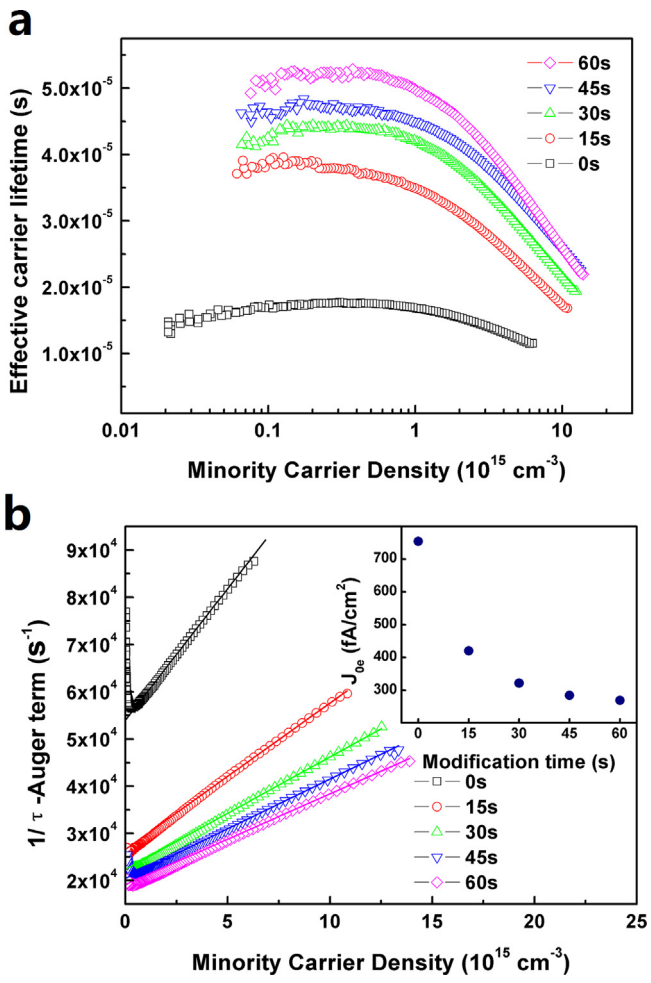

Fig. 4. (a) Minority carrier lifetimes and (b) Auger corrected inverse effective lifetime as a function of injection level for nanotextured surface silicon with TMAH modification for 0 s, 15 s, 30 s, 45 s, and 60 s. The samples are presented in Table 1. The solid line is the tangent line at the injection point to determine the saturation current density. The variation of saturation current densities as a function of modification time is shown in the inset of (b).

modification time within 60 s. It clearly shows that S_{eff} decreases with the increase of modification time within 60 s. The variation of S_{eff} as function of modification time reduces as modification time increases.

As shown in Fig. 5, it was found that the value of S_{loc} decrease from 185 cm/s to 127 cm/s after 15 s TMAH modification, and then decrease to 112 cm/s after another 15 s. This result confirmed our assumption that the increase of τ_{eff} is due to both of the reduction of surface area and the suppression of Auger recombination in emitter by TMAH modification. The value of S_{loc} does not change significantly with the increase in the modification time to 45 s. Our results showed that the optimized modification time is around 30 s, at this time, the P dopant concentration was significantly reduced. The value of S_{loc} increased to 132 cm/s with 60 s TMAH modification, which is due to non-uniformity in the surface emitter for the over surface etching.

Table 1 shows the open circuit voltage (V_{OC}), short circuit current density (J_{SC}), fill-factor (FF), and efficiency (η) of group S1, group S2, group S3 and the group R measured under AM 1.5G. We found that the V_{OC}, J_{SC} and η of the group S2 were enhanced 16.35 mV, 1.34 mA/cm^2 and 1.16% (absolute) compared with group S1, though group S2 showed lower reflectance. A high V_{OC} was achieved due to (a) the reduced surface recombination owing to

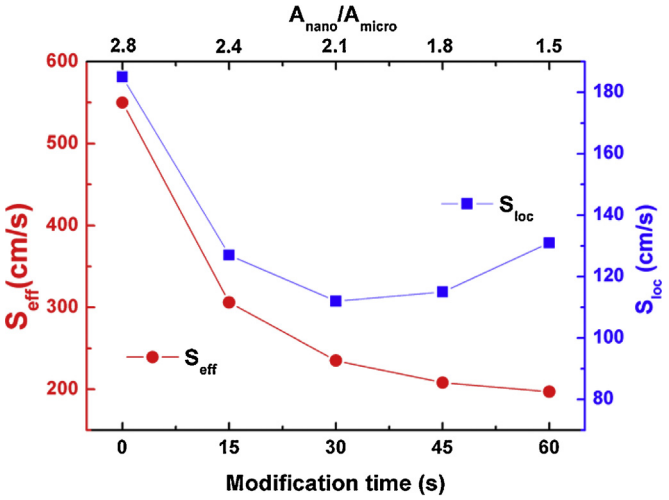

Fig. 5. Evaluation of S_{eff} (left y-axis) and S_{loc} (right y-axis) as a function of TMAH modification time (bottom x-axis) and A_{Nano}/A_{Micro} (top x-axis).

Table 1
Summary of the average electrical parameters of reference solar cells (R), nanotextured solar cells without any modification (S1), nanotextured solar cells with 30 s TMAH modification (S2) and nanotextured solar cells with 60 s TMAH modification (S3). The average values are calculated from 5 to 10 cells.

Group	V_{OC} (mV)	J_{SC} (mA/cm^2)	FF (%)	η (%)
S1	620.38 ± 2.27	36.47 ± 0.33	78.85 ± 0.26	17.84 ± 0.12
S2	636.73 ± 0.36	37.81 ± 0.08	78.92 ± 0.16	19.00 ± 0.04
S3	633.93 ± 2.10	37.43 ± 0.19	77.25 ± 0.30	18.33 ± 0.13
R	636.93 ± 1.20	37.36 ± 0.17	79.09 ± 0.13	18.82 ± 0.11

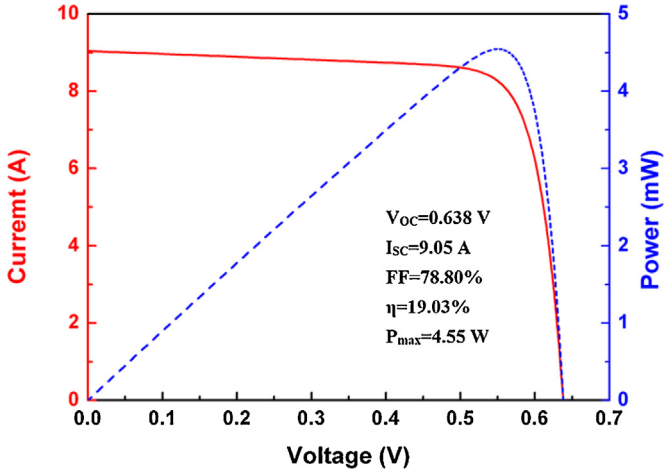

Fig. 6. *I–V* characteristic of the best nanotextured 156 × 156 mm^2 crystalline solar cells.

the decrease in surface area after TMAH modification and (b) the suppression of the Auger recombination in the emitter, which was because of the removal of the "dead layer" using the TMAH solution. This suppression of recombination has positive influence on the passivation of group S2 cells and enhances the collection efficiency of electrons, which results in a higher J_{SC} and η. However, the η of group S3 decreased to 18.33% due to the slightly decrease in V_{OC}, J_{SC} and the sharply decrease in FF. The decrease of J_{SC} could be attributed to the reduction of absorption at surface region for the excessively etching time. The low fill factor was caused by the increase in the series resistance owing to the high sheet resistance (over 120 Ω/□). We also prepared an industry-standard mono-crystalline solar cell with pyramid-textured surface, and the electrical performance was presented in Table 1. The J_{SC} and η of our best black silicon solar cells with TMAH modification are higher than those of the industrial-standard mono-crystalline solar cell, which could be attributed to the lower reflectance of the black silicon solar cells. A nanotextured silicon solar cells has achieved a 19.03% (V_{OC} = 0.638 V, J_{SC} = 9.05 A, FF = 78.80%) efficiency on 156 × 156 mm^2 crystalline silicon wafer. The *I–V* characteristic is shown in Fig. 6.

Fig. 7 shows the IQE of the group S1, S2, S3 and R as a function of wavelength range between 350 and 1100 nm. It also shows an appreciable difference in the wavelength range between 350 and 650 nm between the group S1 and others. The higher dopant concentration in the emitter of group S1, increases the photons absorbed in the emitter and space charge region, which corresponds to an incident wavelength between 350 and 650 nm [14]. The IQE of group S2 and group S3 were improved in the wavelength range between 350 and 650 nm, suggesting that TMAH modification effectively suppress the emitter carrier recombination. Fig. 7 shows a similar IQE between groups S2 and S3, the IQE was slightly enhanced after additional 30 s TMAH modification. Compared to standard pyramid-textured solar cells (group R), the nanotextured

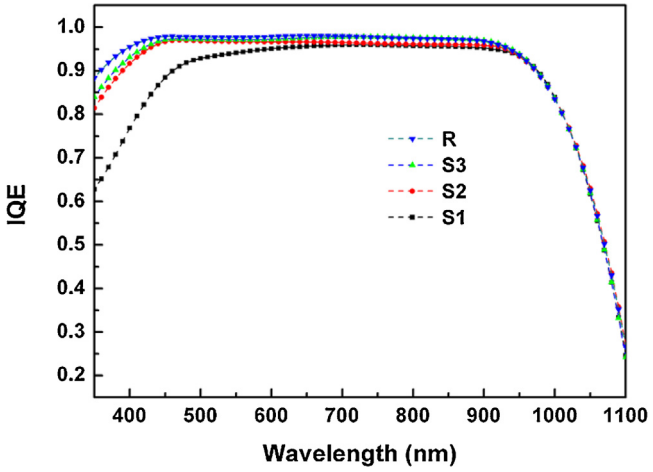

Fig. 7. Internal quantum efficiency of reference solar cell, and solar cells that were nanotextured without TMAH modification and that were nanotextured with TMAH modification for 30 s and 60 s.

solar cells subjected to TMAH modification (groups S2 and S3) have lower IQE in the wavelength between 350 and 450 nm, because of the enhanced surface recombination due to the enlarged surface area.

4. Conclusion

Nano-textured front silicon surface and emitter modification were realized using TMAH solution after phosphorus diffusion. Significant improvements in V_{OC} and J_{SC} were observed leading to increased solar cell efficiency for modified nanotextured surface compared to the traditional nanotextured surface. We found that the Auger recombination in nanotextured emitters is very high because of the high dopant concentration due to the large bare surface region instead of the pyramid-textured surface in diffusion. The TMAH solution is used to reduce the surface area and suppress the Auger recombination in emitter after phosphorus diffusion. An increase of 1.16% in cell efficiency was achieved with a gain of 16.34 mV in V_{OC} and 1.34 mA/cm^2 in J_{SC}. This was achieved by the reduction in the Auger recombination in emitter and the decreases in the surface area. Finally, our best solar cells with nanotextured front surface exhibit higher conversion efficiency than traditional pyramid-textured mono-crystalline silicon solar cells. Nano-textured front surface silicon therefore presents great potential for industrial applications.

Acknowledgements

The authors would like to thank Lili Wang for the SEM measurements and Tao Hu for the EQE measurements. This work is supported by National High-tech R &D Program of China (863 Program) under Grant No.2011AA050516.

References

[1] P. Doshi, G.E. Jellison, A. Rohatgi, Characterization and optimization of absorbing plasma-enhanced chemical vapor deposited antireflection coatings for silicon photovoltaics, Appl. Opt. 36 (1997) 7826–7837.
[2] A. Luque, S. Hegedus, Handbook of Photovoltaic Science and Engineering, John Wiley & Sons, 2011.
[3] H. Nagel, A.G. Aberle, R. Hezel, Optimised antireflection coatings for planar silicon solar cells using remote PECVD silicon nitride and porous silicon dioxide, Prog. Photovolt. 7 (1999) 245–260.
[4] B.G. Prevo, E.W. Hon, O.D. Velev, Assembly and characterization of colloid-based antireflective coatings on multicrystalline silicon solar cells, J. Mater. Chem. 17 (2007) 791–799.

[5] A. Premoli, M.L. Rastello, Minimax refining of wideband antireflection coatings for wide angular incidence, Appl. Opt. 33 (1994) 2018–2024.
[6] H.M. Branz, V.E. Yost, S. Ward, K.M. Jones, B. To, P. Stradins, Nanostructured black silicon and the optical reflectance of graded-density surfaces, Appl. Phys. Lett. 94 (2009) 231121.
[7] S. Koynov, M.S. Brandt, M. Stutzmann, Black nonreflecting silicon surfaces for solar cells, Appl. Phys. Lett. 88 (2006) 203107.
[8] H. Sai, H. Fujii, K. Arafune, Y. Ohshita, Y. Kanamori, H. Yugami, M. Yamaguchi, Wide-angle antireflection effect of subwavelength structures for solar cells, Jpn. J. Appl. Phys. 46 (2007) 3333.
[9] X. Li, P.W. Bohn, Metal-assisted chemical etching in HF/H[sub 2]O[sub 2] produces porous silicon, Appl. Phys. Lett. 77 (2000) 2572.
[10] Y. Cao, A. Liu, H. Li, Y. Liu, F. Qiao, Z. Hu, Y. Sang, Fabrication of silicon wafer with ultra low reflectance by chemical etching method, Appl. Surf. Sci. 257 (2011) 7411–7414.
[11] M. Shen, C.H. Crouch, J.E. Carey, E. Mazur, Femtosecond laser-induced formation of submicrometer spikes on silicon in water, Appl. Phys. Lett. 85 (2004) 5694–5696.
[12] J. Yoo, Reactive ion etching (RIE) technique for application in crystalline silicon solar cells, Sol. Energy 84 (2010) 730–734.
[13] C.C. Striemer, P.M. Fauchet, Dynamic etching of silicon for broadband antireflection applications, Appl. Phys. Lett. 81 (2002) 2980–2982.
[14] J. Oh, H.C. Yuan, H.M. Branz, An 18.2%-efficient black-silicon solar cell achieved through control of carrier recombination in nanostructures, Nat. Nanotechnol. 7 (2012) 743–748.
[15] W.-C. Wang, C.-W. Lin, H.-J. Chen, C.-W. Chang, J.-J. Huang, M.-J. Yang, B. Tjahjono, J.-J. Huang, W.-C. Hsu, M.-J. Chen, Surface passivation of efficient nanotextured black silicon solar cells using thermal atomic layer deposition, ACS Appl. Mater. Interfaces 5 (2013) 9752–9759.
[16] Z. Zhao, P. Li, Y. Wei, C. Lu, X. Tan, A. Liu, 17.3% efficient black silicon solar cell without dielectric antireflection coating, Sol. Energy 110 (2014) 714–719.
[17] D.E. Kane, R.M. Swanson, Measurement of the emitter saturation current by a contactless photoconductivity decay method, in: Proc. 18th IEEE Photovoltaic Specialists Conference (IEEE PVSC), Las Vegas, 1985, pp. 578–583.
[18] T. Mankad, R.A. Sinton, J. Swirhun, A. Blum, Inline bulk-lifetime prediction on as-cut multicrystalline silicon wafers, Energy Proced. 38 (2013) 137–146.
[19] A. Kimmerle, P. Rothhardt, A. Wolf, R.A. Sinton, Increased reliability for J_0-analysis by QSSPC, Energy Proced. 55 (2014) 101–106.
[20] B. Fischer, Loss Analysis of Crystalline Silicon Solar Cells Using Photoconductance and Quantum Efficiency Measurements, Cuvillier, 2003.